JOM Journal of Optical Microsystems

RESEARCH PAPER

Ultrafast ultrasound imaging by optical polymer microring resonator array and a dual optical frequency comb: a theoretical concept

Ahmed S. Bahgat,[a] Jean Provost,[a,b] Denis Seletskiy,[a] and Yves-Alain Peter[a,*]
[a]Polytechnique Montréal, Department of Engineering Physics, Montréal, Québec, Canada
[b]Montréal Heart Institute, Montréal, Canada

ABSTRACT. Ultrasound imaging is typically based on the use of arrays of piezoelectric transducers that can both emit and receive ultrasound. It has recently been shown that on-chip optical microresonator transducers can achieve massive improvements in minimizing footprint and increasing both ultrasound sensitivity and bandwidth; however, the construction of practical arrays remains an open problem. We study the feasibility of making an array of optical microresonators for ultrafast imaging. As a proof of concept, we propose the design of a linear array of polymer microring resonators with equally spaced resonance frequencies. Optical dual-comb setup simultaneously interrogates the whole array's ultrasound perturbation by assigning each microring to a single comb tooth. Using an optical frequency comb for detection provides an efficient way of sampling a large array of transducers while using only a single balanced heterodyne detection scheme per branch.

Keywords: ultrafast ultrasound imaging; polymer microring resonators; optical dual frequency combs; whispering gallery mode; electrooptic modulators

Paper 23021G received Aug. 11, 2023; revised Jul. 1, 2024; accepted Jul. 5, 2024; published Aug. 10, 2024.

1 Introduction

Ultrasound sensors using polymer optical microring resonators (MRRs) and their optical readout received significant attention in the last decade.[1–5] When these MRRs are exposed to ultrasound stimulation, a shift in the resonance frequency is observed due to the change in the microcavity physical parameters. Due to optical resonant enhancement, detection of transmitted/reflected light tuned near the resonance can generally exhibit high sensitivity to an amplitude of the incoming pressure wave, translating to low noise-equivalent pressure. Such resonator-based ultrasound sensors have a wide acoustic bandwidth response, compact footprint, immunity to electromagnetic interference,[4] robust operation, and are poised to potentially exhibit quantum-limited detection capabilities. The next challenge is signal interrogation from an array of sensors. The most common technique for optical detection of the ultrasound signal from a single MRR is a power detection method.[6] In this technique, an optical probe at a fixed optical wavelength is used to interrogate the transmission function of the resonator, where the wavelength of the probe is adjusted to where the on-resonance transmission function varies linearly with wavelength. The shift in the resonator's transmission spectrum due to the ultrasound perturbation causes a variation in the transmitted optical power, which is detected by a high-speed photodiode connected to an advanced oscilloscope system.[1,7] Although this technique is effective when applied

*Address all correspondence to Yves-Alain Peter, yves-alain.peter@polymtl.ca

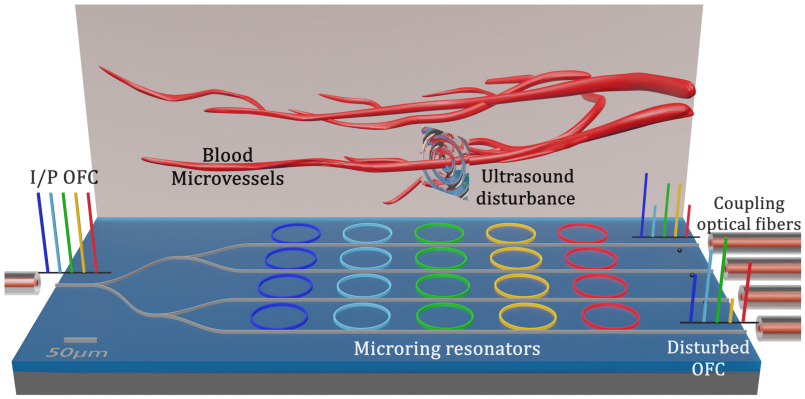

Fig. 1 Schematic of the proposed imaging setup. Ultrasound disturbance (scattering from a tissue) is imaged via an array of optical MRRs. Ultrasound disturbance modulates transmitted light through each spectrally distinguishable resonator, thus providing spectro-spatial multiplexing, enabled by the light-sound interaction and an OFC readout. OFC readout teeth are assigned individually to each MRR in the linear array, as defined by the indicated color code.

to a single laser frequency, it cannot be directly applied to simultaneously read-out signals from an array of MRRs. To achieve such simultaneous readouts, multiple laser sources and corresponding sensors connected to wavelength-division multiplexing are required. However, this approach leads to a bulky and expensive system.[8,9] One of the promising techniques in high-precision multispectral signal interrogation is the optical frequency comb (OFC), in which a spectrum of mutually coherent frequency-equidistant single-mode lasers can be introduced simultaneously. Some researchers introduced digital optical frequency combs (DOFC) spectroscopy in ultrasound detection with materials other than polymers;[8,10,11] however, much research is needed including the integration of OFCs in ultrasound detection and the development of cost-effective materials. Despite the full spectrum given by the DOFC in a certain optical bandwidth, the limited optical bandwidth and crosstalk during demodulation put more constraints on the performance of the microresonator arrays in these techniques.[12]

The schematic of our proposed setup is shown in Fig. 1, where we consider an example of ultrafast imaging of a tissue exposed to an external ultrasound source. A two-dimensional (2D) array of optical MRRs detects ultrasound waves' localized disturbance to construct the dynamic image of blood flow. Ring arrays are arranged in row branches where each ring linear array branch is interrogated with an equally power-split input optical signal and is then coupled to an individual photodiode for signal detection. This design permits an independent and symmetric array design; hence, in this work, we focus primarily on the design of linear arrays. A dual OFC configuration is proposed to be used for parallel signal interrogation in our work. As shown in Fig. 2, consider an example of a linear array of five-ring resonators with different radii, with proposed values in between 50 and 80 μm, $(R_1, R_2, R_3, R_4, R_5)$ having distinguishable transmission spectra and interrogated by OFC modes which are assigned one by one to the resonance of each ring following the power detection method.

Due to a large difference in the periods of optical and ultrasound waves, each comb tooth can be used to resolve microsecond ultrasound dynamics. Then, as shown in Fig. 2, each comb tooth is uniquely overlapped with the corresponding resonance spectrum of MRRs. The resulting spectro-spatial multiplexing can be used to detect the ultrasound excitation of each of them. The readout is accomplished via a reference OFC and with a detuning in the tooth spacing, such that the optical beat frequencies of corresponding tooth pairs can be shifted into the RF baseband for electrical detection. Dual-comb detection configuration allows the spectral response of the ring array to be measured rapidly and without any systematic limitations of conventional techniques.[13]

A schematic of the dual OFC used in our design is shown in Fig. 3. Two coherent laser beams that have slightly different optical frequencies $[f_1, f_2 = (f_1 + \delta f)]$ are fed into two separate identical electro-optic phase modulators (EOMs). To maintain coherence, these two optical frequencies are driven from the same laser source and one branch is frequency shifted by δf using, for example, acousto-optic frequency shifter. EOMs are driven by two RF signals with

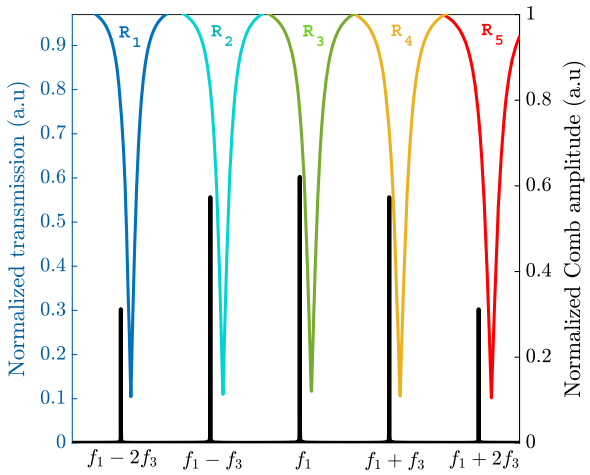

Fig. 2 Example of a five-microring transmission spectrum and corresponding OFC in power detection method mode. Each microring resonance is assigned individually to a single OFC tooth. The demultiplexing of the final readout of the OFC gives the corresponding disturbance at each MRR.

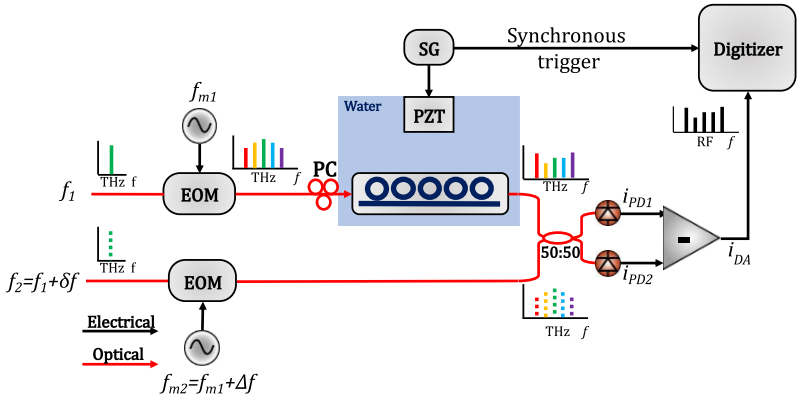

Fig. 3 Schematic of dual-comb interrogation experimental setup of microresonator linear array. OFC, optical frequency comb; EOM, electrooptic modulator; PZT, piezoelectric transducer; SG, signal generator; PC, polarization controller.

a slight RF frequency shift $[f_{m1}, f_{m2} = (f_{m1} + \Delta f)]$ and are generated by a two-tone phase-stabilized RF generator working at the GHz regime (5 to 15 GHz). One of these two combs will act as a local oscillator signal, while the other will be used for signal interrogation of the ring array configuration. To detect the variation in the optical signal due to the ultrasound perturbation, a balanced heterodyne detection scheme is used. In this technique, the interrogated signal is mixed with the local oscillator signal through a (50:50) fiber beam splitter/combiner. Then, the two photodiode currents are differentially amplified to minimize random errors.

This proposed scheme is different from the already introduced DOFC in the literature.[8,12] First, the RF bandwidth f_{bw} of EOMs determines the optical spectral spacing between each two comb teeth, while the number of generated comb teeth n is controlled by the input RF power that defines the total optical bandwidth to be $(n-1) * f_{\mathrm{bw}}$. While in the DOFC technique, the RF bandwidth f_{bw2} of the used electrooptic intensity modulator defines the total optical bandwidth, and the optical spectral spacing between every two teeth is $f_{\mathrm{bw2}}/(n-1)$. This main difference does not force the resonance frequencies of the microring array to fit within a very narrow optical bandwidth f_{bw2} and hence reaching an ultra-high quality factor, while it is better from the sensitivity aspect, is not the limit anymore for increasing the number of elements of the array, like in the case of the DOFC technique.[12] The number of elements will be limited to the number of the generated comb teeth. Furthermore, down-converting the optical band to RF band in the dual-combs scheme makes the detection of these combs an easy task with a common photodiode

bandwidth attached to a common digitizer and reduces processing time and simplifies electronic complexity. Moreover, the introduced comb readout technique provides optical amplification of the detected signals and suppresses crosstalk between the interrogation combs. In this work, we investigated a detailed overview of the theory and design of polymer optical MRR array for acoustic imaging systems and employed the detection technique of optical-dual frequency comb to measure the ultrasound response of the MRR array. A careful choice of both the ring radii and the frequency comb parameters is being introduced to comply with the power detection method of the array simultaneously. An overview of the expected device's performance is also introduced.

2 Theoretical Background

2.1 Ultrasound Detection Mechanism by Microring Resonators

MRR is a type of whispering gallery mode (WGM) resonator that consists of a ring-shaped waveguide, acts as a resonant optical cavity, coupled to a bus waveguide forming optical input and output,[14] Fig. 4(a). The gap between the waveguide and the MRR is on a scale of optical wavelength and tailored to reach critical coupling to achieve high-Q resonances.

If a wideband optical signal is input to the waveguide, then, output intensity resonance dips (output intensity is minimum) occur in the transmission spectrum representing the resonance wavelength λ_r of the WGM resonator and depend mainly on the geometry and waveguide optical parameters. It can be expressed as[15]

$$m\lambda_r = 2\pi R n_{\text{eff}}(\lambda_r, R), \tag{1}$$

where m is the azimuth mode number, R is the radius of the microring, and $n_{\text{eff}}(\lambda_r, R)$ is the effective refractive index (RI) of the guided mode as a function of the resonance wavelength and the ring radius. When exposed to ultrasound perturbation, the microring responds to the ultrasound waves in two manners. First, the ring waveguide is deformed by acoustic pressure that changes the shape and optical field distribution. This waveguide deformation is remarkable in elastic materials with low Young's moduli, such as polymers.[16] Second, the optical RI of the material itself is perturbed by the strain induced by acoustic pressure linked to the elasto-optic effect in the material.[17] When the ultrasound perturbation occurs, a detectable time-dependent shift in λ_r can be measured, as shown in Fig. 4(b), and is given as

$$\frac{\Delta\lambda_r}{\lambda_r} = \frac{\Delta l}{l} + \frac{\Delta n_{\text{eff}}}{n_{\text{eff}}}, \tag{2}$$

where l and Δl are the length of the resonator, which is the microring circumference, and the induced change in the length, respectively. The sensitivity S of the ultrasound sensor is a key parameter in evaluating the performance of the ultrasound detector. It is defined as the change of optical transmission T under the unit acoustic pressure amplitude P and is given as

$$S = \frac{dT}{dP} = \frac{dn_{\text{eff}}}{dP}\frac{d\lambda_r}{dn_{\text{eff}}}\frac{dT}{d\lambda_r}. \tag{3}$$

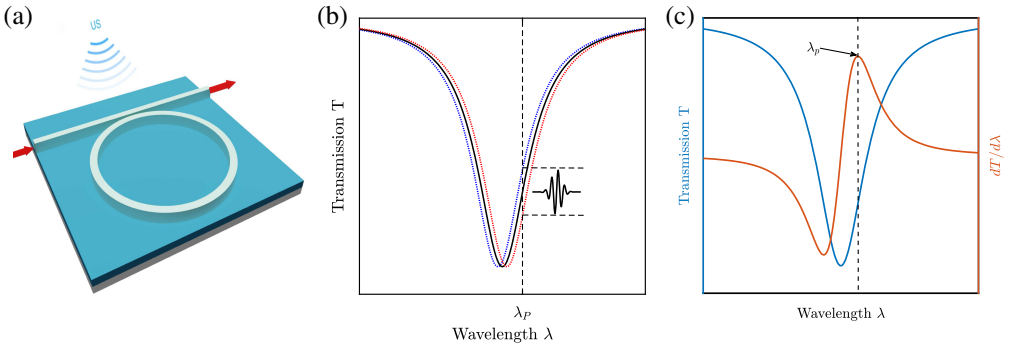

Fig. 4 (a) Microring ultrasonic sensor, (b) ultrasonic signal detection by power-variation method due to optical resonance shift, and (c) the derivative of transmission power with respect to the wavelength λ showing the probing wavelength λ_p at maximum sensitivity.

The first term dn_{eff}/dP represents the change of the RI in the polymer waveguide induced by applied acoustic pressure considering factors, such as Young's modulus, the elasto-optic coefficients of the polymer, and the waveguide's cross-sectional shape. As per the second term $d\lambda_r/dn_{\text{eff}}$, it can be derived from the resonance equation and is given by $2\pi R/m = \lambda_r/n_{\text{eff}}$. Finally, $dT/d\lambda_r$ is the change in transmission associated with λ_r and is defined as the slope of the linear region obtained at the rising or falling edge of the resonance dip. So, as shown in Fig. 4(c), the transmission derivative shows two peaks at the linear parts of the transmission spectrum representing the maximum slope of its linear parts at the rising or falling edges while it is approaching zero value at the other parts of the spectrum.

2.2 Optical Frequency Comb

If we consider an electrooptic phase modulator (EOM) of π optical phase shift voltage of V_π. A continuous wave laser source feeds the EOM at an optical angular frequency ω_o and an electric field amplitude of E_o. The modulator is electrically driven by a sinusoidal waveform using an RF generator at an angular frequency ω_m. The electrical potential is given by $[V(t) = V_o \sin(2\pi f_m t)]$ where V_o is the peak voltage. At the output of the modulator, the optical field experiences a phase shift $[\Delta\varphi = \pi V(t)/V_\pi = \phi_0 \sin(\omega_m t)]$, that controls the output optical field. The time domain representation of the total electric field of the generated comb is given as[18]

$$\tilde{E}(t) = E_0 \sum_{p=-\infty}^{\infty} J_p(\phi_0) e^{i(\omega_0 + p\omega_m)t}, \tag{4}$$

where p is the comb teeth index, and $J_p(\phi_0)$ is Bessel function of order p of a certain constant phase ϕ_0. The frequency domain representation of the generated OFC is described as[18]

$$\tilde{E}(\omega) = E_0 \sum_{=\infty}^{\infty} J_p(\phi_0)\delta(\omega - (\omega_0 + p\omega_m)), \tag{5}$$

From Eq. (5), we see that the modulated signal forms a comb of equidistant laser modes separated by the RF modulation frequency. In addition, the phase amplitude, which depends mainly on V_π, controls the number and the amplitude of the comb teeth following the Bessel function of the first kind J_p. If we consider having two combs that are slightly shifted in frequency by Δf, shown in Fig. 5, one is the local oscillator, and the other is subjected to the ultrasound disturbance function in the form of quadrature Gaussian pulse $G_p(t)$ at each comb index p, then the real term of Eq. (4) for both combs is

$$\begin{aligned} \tilde{E}_1(t) &= E_{01} \sum_{p=-\infty}^{\infty} G_p(t) J_p(\phi_{01}) \cos((\omega_1 + p\omega_{m1})t), \\ \tilde{E}_2(t) &= E_{02} \sum_{p=-\infty}^{\infty} J_p(\phi_{02}) \cos((\omega_2 + p\omega_{m2})t), \end{aligned} \tag{6}$$

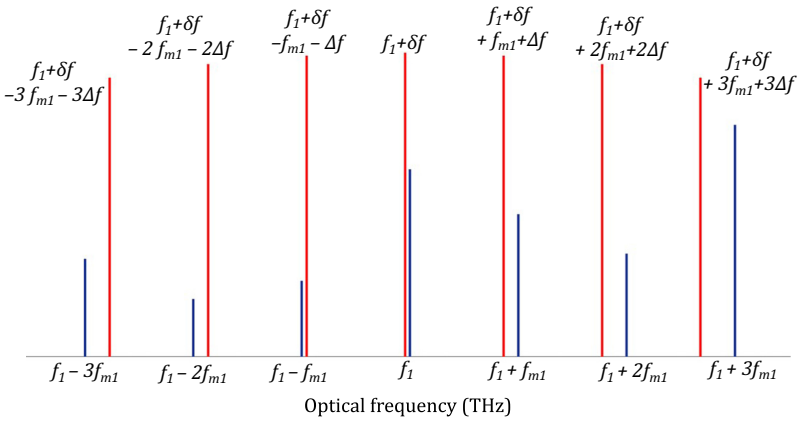

Fig. 5 Optical frequency domain of optical dual-combs, red: local oscillator comb, blue: signal interrogation comb.

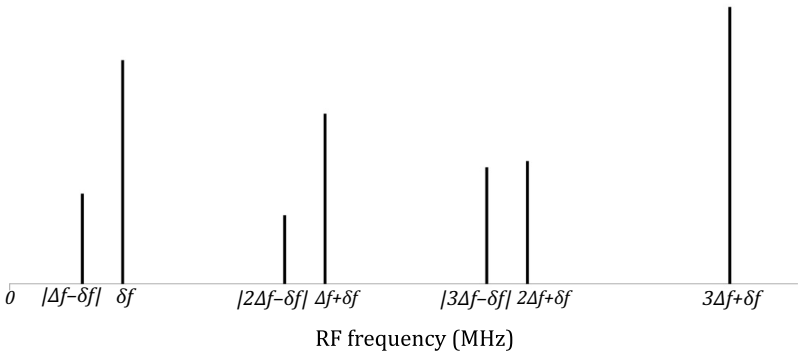

Fig. 6 RF domain down-converted beat frequency between every two pairs of the dual-comb teeth.

where ω_1, ω_2, ω_{m1}, and ω_{m2} are the angular frequencies of corresponding optical and RF frequencies f_1, f_2, f_{m1}, and f_{m2}, respectively. Interfering the two electric field components in the fiber beam combiner results in two complementary signals at each output branch. Each optical signal contains a DC component, a beat frequency at a difference of line-to-line frequencies (shown in Fig. 6), and a high frequency (addition of line-to-line frequencies). Due to its electronic bandwidth limitation, the photodiode only responds to the first two signal contributions, namely the DC component and the beat frequency. Suppose that there is an equal splitting ratio and that the photodiode responsivities are matched $\mathbb{R}$. In that case, the differential amplifier will eliminate the DC components, and only a combination of the beat frequencies is observed. Finally, the output current of the differential amplifier with gain A is given in Ref. 19, while taking a discrete number of comb teeth $(2N+1)$

$$\begin{aligned} i_{\mathrm{DA}} &= 2A\mathbb{R}E_{01}E_{02}\sum_{p=-N}^{N} G_p(t)J_p(\phi_{01})J_p(\phi_{02})\cos((\omega_1 + p\omega_{m1} - \omega_2 - p\omega_{m2})t) \\ &= 2A\mathbb{R}E_{01}E_{02}\sum_{p=-N}^{N} G_p(t)J_p(\phi_{01})J_p(\phi_{02})\cos(2\pi|p\Delta f \pm \delta f|t). \end{aligned} \tag{7}$$

Analysis using the down-conversion to zero-baseband technique[20] is done in Eq. (7) for the extraction of the time-varying $G_p(t)$ ultrasound signal of each comb tooth of index p. In this technique, the acquired time-domain sampled signal is shifted every time by $e^{-i2\pi|p\Delta f \pm \delta f|t}$ with different p, so each time a different comb tooth with index p is centered at zero frequency. Analysis of one comb tooth with index $p = 0$ is being introduced and it is the same analysis techniques for the rest of the comb teeth. Then, the shifted voltage signal is expressed as

$$v_{\mathrm{DA}}(t) = CG_0(t)J_0(\phi_{01})J_0(\phi_{02}) + C\sum_{p=-N}^{N,N\neq 0} G_p(t)J_p(\phi_{01})J_p(\phi_{02})\cos(2\pi|p\Delta f \pm 2\delta f|t), \tag{8}$$

where C is a constant combining the constant terms including the load resistance R. Applying low pass (LP) filter, set to match the acoustic bandwidth, will remove the higher frequency terms which are given by the summation term in Eq. (8). The acoustic signal $\tilde{G}_0(t)$ of this carrier frequency can then be expressed as

$$\tilde{G}_0(t) = \frac{\tilde{v}_{DA}(t)}{CJ_0(\phi_{01})J_0(\phi_{02})}, \tag{9}$$

where $\tilde{v}_{\mathrm{DA}}(t)$ is the filtered measured signal. Band pass (BP) filtering can be used to narrow the detection acoustic bandwidth and to reduce the noise.

3 Design and Simulation

3.1 Microring Array

Toward the experimental realization of our concept, we propose a design focus on a C-band tunable laser source and electrooptic modulators operating around 1550 nm, ensuring low-cost and efficient performance associated with the C-band optics. Nanoimprinted polystyrene is used as the device layer that has an RI ≈ 1.57 [21] at the working wavelength. A thin layer of PDMS is considered for top cladding to isolate the fabricated devices from any contaminants in the measurement medium, usually water, that will improve the device performance while minimizing acoustic reflection loss as the acoustic impedance of PDMS matches the water impedance.[22] The bottom cladding material is a 5 μm-thick silicon wet thermal oxide layer. The waveguide cross-section is a rectangle of 1.4 μm $\times$ 2.0 μm, guaranteeing single-mode operation at the working wavelength. The nanoimprinting technique consists of two crucial steps: 1) fabrication of a hard silicon mold using a well-developed fabrication process that can reach down to 10 nm critical dimension, and 2) transferring the silicon mold patterns to the polystyrene material using the nanoimprinting machine. Due to this nanoimprinting fabrication technique, a 100 nm-thick residual layer of PS was considered in the calculation. Using a finite element method solver, the effective RI of the rings for TE-mode was extracted as a function of the bending radii within a 6 nm optical wavelength range, as shown in Fig. 7. As we introduced before, we use each OFC tooth and assign it to one of the side slopes for each MRR's spectrum. This condition challenged the choice of the ring resonances to be spectrally equally spaced by Δf_2 and a quality factor that guarantees at least a resonance optical bandwidth of $\Delta f_2/2$. In addition, the optical resonance 3 dB bandwidth (δf_o) should be greater than half of the frequency spacing between the comb teeth, i.e., ($\delta f_o \leq f_m/2$), to comply with the power detection method limitations.[6] Reducing the optical resonance 3 dB bandwidth (δf_o) requires the attainment of high-quality factor Q resonances that can be achieved by reaching the critical mode coupling condition and controlling the surface roughness in nanoimprinting mold fabrication.[2–4,23,24] The proposed minimum quality factor to comply with our design is set to 5×10^4 which can be achieved with the proposed fabrication technique and the working optical wavelength by controlling the coupling gap between the MRRs and the bus waveguide.

For acoustic imaging, the standard spatial resolution for acoustic frequency range $f_{\text{acoustic}} = 1 \sim 10$ MHz limits the spacing between the geometrical centers of the rings to be one acoustic wavelength for the highest frequency (≈ 150 μm), and hence it defines the upper limit of the radii of the rings. In addition, the smaller the radius, the higher the optical bend loss, which limits the quality factor Q; hence it defines the lower rings' radii limit to be ≈ 60 μm. Considering the

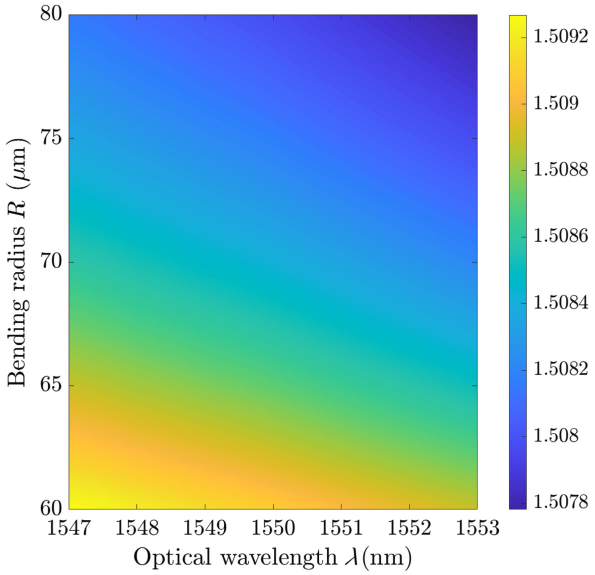

Fig. 7 Extracted effective index of the polymer waveguide at different bending radii using RSoft Femsim. Color bar: effective RI of the waveguide.

Table 1 Matlab script results of five rings' radii following the detection criterion.

R (μm)	Azimuthal index (m)	Resonance frequency (THz)	Δf (GHz)	Q
70.5	431	193.5194	—	5.01×10^4
71.15	435	193.5289	9.5	5.06×10^4
1.80	439	193.5384	9.5	5.11×10^4
72.45	443	193.5478	9.4	5.15×10^4
73.1	447	193.5572	9.4	5.20×10^4

resonance condition [Eq. (1)], there are multiple dependent variables that we need to choose carefully to achieve these resonances, in return providing great control for tailoring the optical design to the specifics of the imaging application. A custom algorithm using MATLAB software was then used to optimize all the parameters in the resonance equation to extract the ring radii that have the exact spectral spacing in the resonance frequencies. Table 1 gives an example of five rings with a ≈ 9.4 GHz resonance spectral spacing with free spectral range (FSR) of ≈ 3.2 nm to ensure that each resonance in the interrogation bandwidth comes from different ring radii, taking into account the fabrication process limitation (we considered 50 nm as our critical dimension) of the nanoimprinting mold while using the electron beam lithography for patterning hard mask. Experimentally, FSR values are not exactly the same for all the microrings due to the small change between the ring radii. Distinguishing these slightly different values of FSR, during the resonance characterization step, enables checking the corresponding resonance spectrum related to each microring. This information will help during the final image construction as we will discuss in Sec. 3.2.

To have an overview of the sensor sensitivity described in Eq. (3), the first two terms can be either simulated or calculated to estimate the sensitivity. COMSOL multiphysics simulation is used to extract the first term by calculating the effective index of refraction for various applied mechanical pressure representing the ultrasound perturbance. Figure 8 shows the extracted simulation results and a linear fit that gives this term to be $dn_{\text{eff}}/dP = -7.897 \times 10^{-5}$ MPa^{-1} for an acoustic pressure range of 0 to 4 MPa.[16,25] As per the second term $d\lambda_r/dn_{\text{eff}}$, it is $\approx 1.032\,\mu$m, for the first ring, as an example. So with the current design parameters, the spectral sensitivity is calculated as $d\lambda_r/dP = (-7.897 \times 10^{-5}\ \text{MPa}^{-1}) \times (1.032\ \mu\text{m}) \approx -81.50$ pm/MPa.

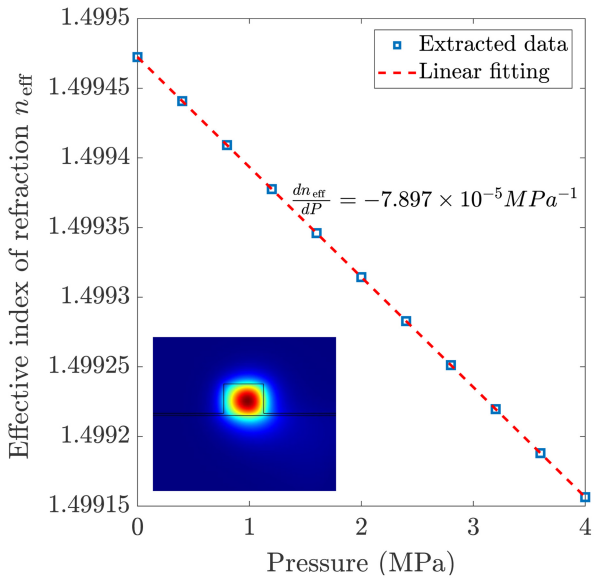

Fig. 8 Extracted effective index of the polymer waveguide when exposed to acoustic pressure. Inset: calculated electric field distribution of TE mode.

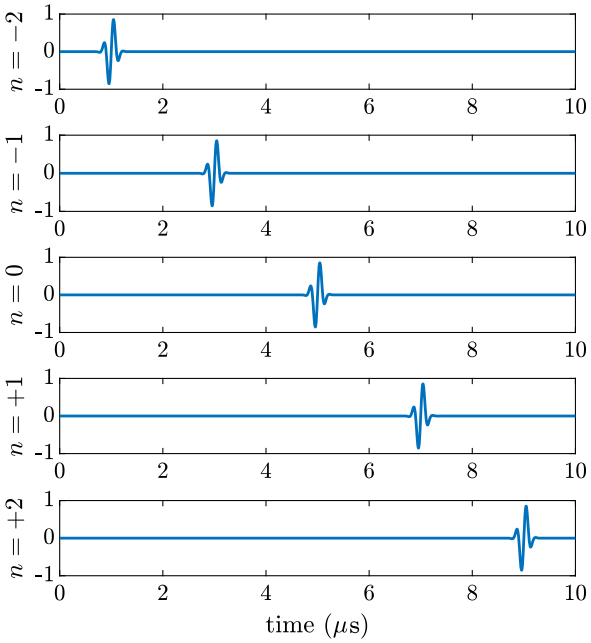

Fig. 9 Representation of the simulated ultrasound pulses assigned to each ring resonator.

3.2 Simulated Interrogation of Ultrasound Signals

EOMs can be adjusted based on the exact spacing between the ring resonators and within their optical bandwidth. As shown in Table 1, the average spectral spacing between the rings' resonances is 9.43 GHz which defines f_m. Δf, δf are to be chosen to be 90 and 20 MHz respectively, based on the photodiode electronic bandwidth and the frequency of the detected ultrasound that leads to five carrier frequencies in the down-converted signal 20, 70, 110, 160, and 200 MHz. We proposed to measure an ultrasound pulse at a center frequency of 5 MHz and a bandwidth of approximately 80%. The proposed photodiodes have an electrical bandwidth of 500 MHz. Let us consider the scattered ultrasound signal from a certain source is represented by a series of ultrasound pulses that have a certain propagation delay as shown in Fig. 9. Figure 10 shows the simulated detected ultrasound demonstrated by optical power variation on each comb tooth representing its corresponding MRR. Fourier transform of the simulated signal that represents the expected output signal from the heterodyne detection after ultrasound disturbance as

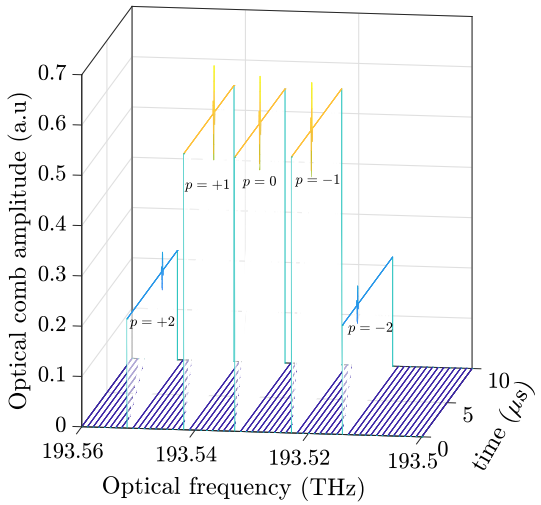

Fig. 10 Representation of the power variation of the five OFCs subjected to ultrasound disturbance over a simulation time interval of 10 μs from the MRR array.

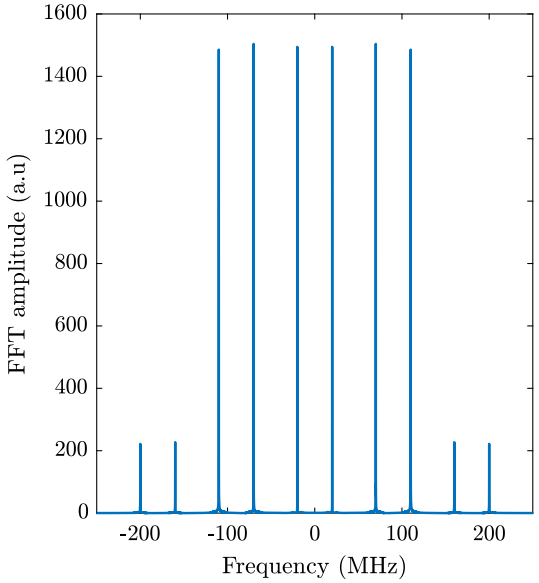

Fig. 11 Fourier transform representation of the simulated signal.

measured by the electronic digitizer is shown in Fig. 11. We extracted each ultrasound pulse signal from its corresponding carrier RF frequency by shifting the whole frequency spectrum to the zero baseband of each carrier frequency. The signal is extracted then by applying a Butterworth low-pass filter with order 5 and bandwidth of 20 MHz. A band-pass infinite impulse response filter is used to reduce any noise coming from any sources out of the acoustic transmitter bandwidth. The filtered bandwidth is as narrow as the ultrasound transducers which is in the range of ± 2 MHz. Figure 12 shows the final filtered signal corresponding to the detected acoustic disturbance by the ring resonators array, which is delayed in correspondence to the arrival time of the acoustic wave on each individual element (i.e., ring resonator). These detected delays will be further used for the image construction. This technique offers no limitation on the detected ultrasound frequency as long as sufficient sampling can be achieved.

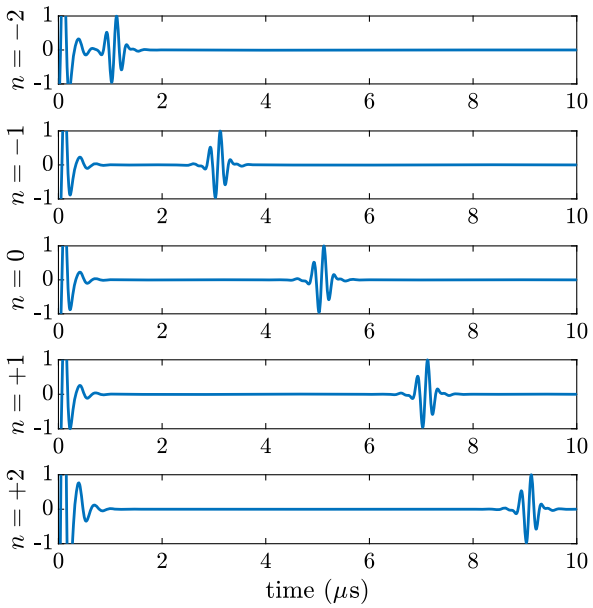

Fig. 12 The filtered signal from all the carrier frequencies after applying down-conversion to zero baseband method.

4 Discussion

Adding experimental insight, careful polarization control during experiments should be considered, as the given optimization parameters for the design are only for the chosen TE-mode. The other supported single mode (i.e., TM-mode) has effective refractive indices that differ from the extracted values for TE-mode, Fig. 7, and hence the designed array will have a completely different spectrum.

In addition, the resonance frequencies and the quality factors given by the theoretical optimization method may be affected by any variations imposed by fabrication uncertainties.[12] However, the tunable nature of the introduced dual OFC can overcome these variations if the resonance spacing between each pair of rings is still within the working optical bandwidth of the electrooptic modulator. Furthermore, the ultrasound disturbance can be detected from either side of the resonance slopes, which provides a good opportunity for the tunability of the dual OFC to succeed within a reasonable sensitivity range around the probing wavelength λ_p. Another possible solution is taking into consideration the thermooptic coefficient of the suggested polystyrene material to retune the resonance spectrum by tuning the index of refraction of each ring using localized heaters.[26,27]

The MMRs are known for their wider acoustic bandwidth, theoretically a few hundred MHz, limited only by the thickness of the device layer making it suitable for high-frequency applications, such as photoacoustics. The dual OFC technique can be also tuned to fit with these high frequencies by choosing the right parameters for Δf and δf by the relation $|p\Delta f \pm \delta f|$, which defines the carrier frequencies. δf is constrained by the available commercial optical frequency shifters while we have full control to choose Δf taking into consideration our photodiode and digitizer electrical bandwidth. The maximum acoustic bandwidth is limited to half of the frequency difference between each two consecutive carrier frequencies in the RF domain.

The proposed dual OFC technique provides flexibility in detection as the RF bandwidth of EOMs determines the spacing between the generated comb teeth, while the parameter V_π controls the number of comb teeth generated at a certain input RF power, so that, the theoretical maximum number of simultaneously detected MRRs is only limited by the number of frequency comb teeth that can be generated. Furthermore, as discussed before, the minimum quality factor is limited by $f_m/2$ that does not impose unachievable restrictions on the performance of MRRs, which are expected to be primarily affected by fabrication uncertainties.

5 Conclusion

In conclusion, a complete insight into ultrasound detection using MRRs and parallel interrogation using dual OFCs generated by EOMs was introduced. The performance aspects of the MRRs, as well as the dual OFCs, were introduced. The discussed techniques provided an efficient way for ultrasound imaging in both slow-acting or ultrafast phenomenon in biomedical tissue. OFC-based techniques provide high signal-to-noise ratios, enabling sensitive optical measurements of the resonators' spectrum. The ultrafast nature of OFCs allows real-time assessment of tissue motion and visualization of rapid physiological events, such as 3D volumetric blood flow dynamics, cardiac function, and tissue elasticity.

Disclosures

The authors declare no conflicts of interest.

Code and Data Availability

All data in support of the findings of this paper are available within the article.

Acknowledgments

A.S.B. was financially supported by the Egyptian Ministry of Defense. The authors acknowledge support from the Fonds de recherche du Québec-Nature et technologies (FRQNT)-Projet de recherche en équipe 2022-PR-300761, CMC Microsystems-MNT Program, and the Natural Sciences and Engineering Research Council of Canada-Discovery grants.

A.S.B. would like to thank Cédric Lemieux-Leduc, Marc-Antoine Bianki, Régis Guertin, Thomas Lacasse, and Salvador Poveda-Hospital for stimulating discussions and valuable suggestions.

References

1. A. Maxwell et al., "Polymer microring resonators for high-frequency ultrasound detection and imaging," *IEEE J. Sel. Top. Quantum Electron.* **14**(1), 191–197 (2008).
2. T. Ling, S.-L. Chen, and L. J. Guo, "Fabrication and characterization of high q polymer micro-ring resonator and its application as a sensitive ultrasonic detector," *Opt. Express* **19**, 861–869 (2011).
3. C. Zhang et al., "Review of imprinted polymer microrings as ultrasound detectors: design, fabrication, and characterization," *IEEE Sens. J.* **15**(6), 3241–3248 (2015).
4. C. Zhang et al., "Imprinted polymer microrings as high-performance ultrasound detectors in photoacoustic imaging," *J. Lightwave Technol.* **33**(20), 4318–4328 (2015).
5. C. Zhang et al., "Ultrabroad bandwidth and highly sensitive optical ultrasonic detector for photoacoustic imaging," *ACS Photonics* **1**(11), 1093–1098 (2014).
6. C.-Y. Chao, W. Fung, and L. Guo, "Polymer microring resonators for biochemical sensing applications," *IEEE J. Sel. Top. Quantum Electron.* **12**(1), 134–142 (2006).
7. T. Ling, S.-L. Chen, and L. J. Guo, "High-sensitivity and wide-directivity ultrasound detection using high Q polymer microring resonators," *Appl. Phys. Lett.* **98**(20), 204103 (2011).
8. J. Song et al., "Ultrasound measurement using on-chip optical micro-resonators and digital optical frequency comb," *J. Lightwave Technol.* **38**(19), 5293–5301 (2020).
9. G. Wissmeyer et al., "Looking at sound: optoacoustics with all-optical ultrasound detection," *Light: Sci. Appl.* **7**(1), 53 (2018).
10. J. T. Friedlein et al., "Dual-comb photoacoustic spectroscopy," *Nat. Commun.* **11**(1), 3152 (2020).
11. J. Pan et al., "Microbubble resonators combined with a digital optical frequency comb for high-precision air-coupled ultrasound detectors," *Photonics Res.* **8**, 303–310 (2020).
12. J. Pan et al., "Parallel interrogation of the chalcogenide-based micro-ring sensor array for photoacoustic tomography," *Nat. Commun.* **14**(1), 3250 (2023).
13. I. Coddington, N. Newbury, and W. Swann, "Dual-comb spectroscopy," *Optica* **3**, 414–426 (2016).
14. T. J. Kippenberg and K. J. Vahala, "Cavity opto-mechanics," *Opt. Express* **15**(25), 17172–17205 (2007).
15. J. Heebner, R. Grover, and T. Ibrahim, *Optical Microresonator Theory*, Springer (2008).
16. H. Li et al., "A transparent broadband ultrasonic detector based on an optical micro-ring resonator for photoacoustic microscopy," *Sci. Rep.* **4**(1), 4496 (2014).
17. B. E. Saleh and M. C. Teich, *Fundamentals of Photonics*, John Wiley & Sons (2019).
18. A. Parriaux, K. Hammani, and G. Millot, "Electro-optic frequency combs," *Adv. Opt. Photonics* **12**, 223–287 (2020).
19. M. Seimetz and C.-M. Weinert, "Options, feasibility, and availability of 2 00d7 4 9000B0 hybrids for coherent optical systems," *J. Lightwave Technol.* **24**, 1317 (2006).
20. S. K. Mitra, *Digital Signal Processing: A Computer-Based Approach*, McGraw-Hill Higher Education (2001).
21. X. Zhang et al., "Complex refractive indices measurements of polymers in visible and near-infrared bands," *Appl. Opt.* **59**, 2337–2344 (2020).
22. F. Sabri et al., "*In vivo* ultrasonic detection of polyurea crosslinked silica aerogel implants," *PLoS One* **8**, e66348 (2013).
23. X. Tu et al., "Ultrahigh Q polymer microring resonators for biosensing applications," *IEEE Photonics J.* **11**(2), 4200110 (2019).
24. H. Li et al., "Disposable ultrasound-sensing chronic cranial window by soft nanoimprinting lithography," *Nat. Commun.* **10**(1), 4277 (2019).
25. C.-Y. Chao et al., "High-frequency ultrasound sensors using polymer microring resonators," *IEEE Trans. Ultrason. Ferroelectr. Freq. Control* **54**(5), 957–965 (2007).
26. Z. Zhang et al., "Thermo-optic coefficients of polymers for optical waveguide applications," *Polymer* **47**(14), 4893–4896 (2006).
27. S. T. Ilie et al., "Thermo-optic tuning of silicon nitride microring resonators with low loss non-volatile Sb_2S_3 phase change material," *Sci. Rep.* **12**(1), 17815 (2022).

Ahmed S. Bahgat received his PhD in engineering physics from Polytechnique Montréal in 2023. He received his BEng degree in electrical engineering and his MSc degree in engineering physics from Military Technical College in 2011 and 2018, respectively. His current research interests include optical microresonators in sensing, microfabrication, and nonlinear optics.

Jean Provost is the IVADO associate professor of engineering physics at Polytechnique Montréal, Canada. He is a graduate of Polytechnique Montreal and Ecole Centrale Paris and obtained his PhD from Columbia University in 2012. He then became a Marie Curie Fellow and research scientist at Institut Langevin in Paris from 2012 to 2018. In 2018, he joined Polytechnique Montréal where his research focuses on the development of novel ultrasound technologies.

Denis Seletskiy is an associate professor at the Department of Engineering Physics, Polytechnique Montréal and a Canada Research Chair in "Ultrafast and Quantum Photonics." He received his PhD in optical science and engineering from the University of New Mexico in 2010. He held a National Research Council Associateship (2010–2012) at the Air Force Research Laboratory and a Marie-Curie Zukunftskolleg fellowship (2014–2017) at the University of Konstanz. Since 2017, he has led the femtoQ lab in time-domain quantum optics.

Yves-Alain Peter is currently a professor in the Department of Engineering Physics, Polytechnique Montréal. He received his MSc degree in physics and his DrSc degree from the University of Neuchãtel, Switzerland, in 1994 and 2001, respectively. In 1995, he joined the Department of Medical Radiobiology, Paul Scherrer Institute, Switzerland, as a research associate. From 1995 to 2001, he was a graduate research assistant with the Applied Optics Group, Institute of Microtechnology, University of Neuchãtel. From 2001 to 2003, he was a post-doctoral researcher with the Microphotonics Group, Stanford University. From 2003 to 2004, he was a research and development engineer and a project leader with the Swiss Center for Electronics and Microtechnology, Switzerland. In 2004, he joined Polytechnique Montréal, Canada. His current research interests include microphotonics and micro-opto-electro-mechanical systems.